THESIS FOR THE DEGREE OF DOCTOR OF PHILOSOPHY IN SOLID AND STRUCTURAL MECHANICS

Poromechanical Modeling of Composites Manufacturing

MOHAMMAD S. ROUHI

Department of Applied Mechanics
Division of Material and Computational Mechanics
CHALMERS UNIVERSITY OF TECHNOLOGY

Göteborg, Sweden 2015

Poromechanical Modeling of Composites Manufacturing
MOHAMMAD S. ROUHI
ISBN 978-91-7597-144-5

Doktorsavhandlingar vid Chalmers tekniska högskola
Ny serie nr. 3825
ISSN 0346-718X
Department of Applied Mechanics
Division of Material and Computational Mechanics
Chalmers University of Technology
SE-412 96 Göteborg
Sweden
Telephone: +46 (0)31-772 1000

Cover:
Holistic modeling of composites manufacturing

Chalmers Reproservice
Göteborg, Sweden 2015

Poromechanical Modeling of Composites Manufacturing
Thesis for the degree of Doctor of Philosophy in Solid and Structural Mechanics
MOHAMMAD S. ROUHI
Department of Applied Mechanics
Division of Material and Computational Mechanics
Chalmers University of Technology

Abstract

Fibre reinforced composite materials are used extensively in today's industry. On one hand, the low–weight feature of this kind of material gives important advantages such as better fuel efficiency and lower amount of CO2 emissions. On the other hand, high strength and corrosion resistance has made them suitable for different applications. Composite materials are also assumed to grow significantly in automotive industry in near future. In these perspectives, especial attention has risen up towards development of advanced manufacturing technologies where higher production rate, lower cost and lower environmental issues are desired. To achieve this goal, numerical simulations and CAE tools are employed to predict the behavior of manufacturing methods with respect to the process optimization and the product properties.

The focus of this research thesis is toward development of a framework for holistic modeling of fiber reinforced composites manufacturing. The manufacturing process can be considered as a fluid filled porous material, which can be described, on macro scale as well as micro scale, by the Theory of Porous Media (TPM). The TPM has been further enhanced by introducing the concept of phase compressibility of the biphasic mixture of solid and fluid, in order to describe the physical sub–processes happening in different scale. The model of the considered problem is then put forward to be solved by Finite Element Method (FEM). In the discretization of the numerical domain a quadratic six–node triangular element is used and a staggered solution procedure is chosen to solve the highly coupled problem in a finite strain regime. The most important challenges, that the numerical solution procedure is able to capture, are (1) modeling the compressible volumetrically–deformable fiber preform and the shape of membrane due to the different considered loading situations (2) the dual scale resin flow motion through the fibrous preform and the compaction of individual plies (3) deformation dependent permeability models (4) the free surface problem when the flow is moving with respect to a flow front velocity into the vacuum zone of the porous material.

The framework that is developed here is capable of simulating different manufacturing processes based on the chosen initial conditions, boundary conditions and material parameters. Liquid Composite Molding (LCM), Liquid Resin Infusion (LRI), Resin Transfer Molding (RTM), Out of Autoclave (OoA), press forming prepregs, Engineering Vacuum Channels (EvaC) and similar manufacturing methods are some examples of the processes that have been simulated.

Keywords: Poromechanics; Finite element Analysis (FEA); Polymer Composites; Composites Manufacturing

to my beloved family

Preface

The work presented in this thesis is carried out at the department of Applied Mechanics, division of Material and Computational Mechanics at Chalmers University of Technology during January 2011–January 2015. The work is also partly funded and carried out at the Swedish Research Institute of Composite Material, Swerea SICOMP, from February 2012.

I would like to take this opportunity to express my sincere gratitude to my supervisor Professor Ragnar Larsson, whom has given excellent supervision, always ready to discuss and give input to the work as well as read and give feedback on manuscripts.

I am also very grateful to my co–supervisor Assistant Professor Maciej Wysocki for his support and guidance during this project. His knowledge on composite materials has been a great source in the course of this work. He has always been kind and helpful which has made all the conversations and discussions more fun.

I would also like to thank my colleagues at Chalmers and also at Swerea SICOMP for pleasant time and friendly environment they provided.

The last but not least, I am grateful to my lovely wife, Parisa, for all her love and support. She has made my life full of joy and happiness. Her presence and patience was encouraging all the time. I love you.

Mohammad S. Rouhi
January 2015

Acknowledgements

I hereby acknowledge Chalmers University Area of Advance: Material Science, SICOMP Foundation and European Union (via FP7 project ENLIGHT under the Grant 314567), The Swedish Research Council, SAFER – Vehicle and Traffic Safety Centre at Chalmers University of Technology for supporting part of this research.

Thesis

This thesis consists of an extended summary and the following appended papers:

Paper A Larsson R. Rouhi, M.S., Wysocki, M., Free surface flow and preform deformation in composites manufacturing based on porous media theory, European Journal of Mechanics A/Solids 31 (2012) 1–12.

Paper B Rouhi, M.S., Wysocki, M., Larsson, R., Modeling of coupled dual–scale flow–deformation processes in composites manufacturing, Journal of Composites Part A 46 (2013) 108—116.

Paper C Rouhi, M.S., Wysocki, M., Larsson, R., Experimental assessment of coupled dual–scale flow–deformation processes in composites manufacturing, submitted to Journal of Composites Part A.

Paper D Rouhi, M.S., Larsson, R., Wysocki, M., Holistic modeling of composites manufacturing using poromechanics, to be submitted to European Journal of Mechanics A/solids.

The appended papers were prepared in collaboration with co–authors. The author contribution in to the appended papers is described here.

Paper A The author was responsible for planning the paper, writing part of the paper, adapting the developed theory of porous media to enhance the continuum formulation for Liquid Resin Infusion (LRI) manufacturing methods, development of the new part of the numerical implementation and carrying out numerical simulations.

Paper B The author was responsible for planning and writing the paper, adapting the developed theory of porous media for Out of Autoclave (OoA) and press forming manufacturing methods, development of the new part of the numerical implementation and carrying out numerical simulations.

Paper C The author was responsible for planning and writing the paper, optimization of the developed simulation framework in Paper B for Out of Autoclave (OoA) and press forming manufacturing methods, carrying out the numerical simulations and validation and verification against the experimental data.

Paper D The author was responsible for planning and writing the paper, development of the theory and numerical implementation of the formulation and carrying out numerical simulations.

Contents

Abstract i

Preface v

Acknowledgements v

Thesis vii

Contents ix

List of Notations xi

I Extended Summary 1

1 Introduction 1
1.1 Background . . . 1
1.2 Composite materials . . . 1
1.3 Composite manufacturing . . . 2
1.4 Process modeling of advanced composites . . . 3

2 Continuum mechanics of two–phase porous media 4
2.1 Background . . . 4
2.2 The concept of two phase mixture . . . 5
2.3 Conservation of mass . . . 7
2.4 Balance of momentum . . . 8
2.5 Balance of energy . . . 9
2.6 Entropy inequality . . . 11
2.7 Constitutive relations . . . 13
2.8 Numerical implementations . . . 15

3 Summary of Appended Papers 17

4 Conclusion 18

5 Future work 19

References 20

II Appended Papers A–D 21

List of Notations

ϕ^g gas volume fraction , see equation (2.1) 6

ϕ^l liquid volume fraction , see equation (2.1) 6

ϕ^p particles volume fraction , see equation (2.1) 6

ϕ^v voids volume fraction , see equation (2.1) 6

n^f macroscopic volume fractions for the fluid phase, see equation (2.1) 6

n^s macroscopic volume fractions for the solid phase, see equation (2.1) 6

ρ^f_{mic} microscopic intrinsic density for fluid phase , see equation (2.4) 6

ρ^s_{mic} microscopic intrinsic density for solid phase , see equation (2.4) 6

ρ^f macroscopic intrinsic density for fluid phase , see equation (2.4) 6

ρ^s macroscopic intrinsic density for solid phase , see equation (2.4) 6

ρ^f_0 intrinsic density for fluid phase in reference configuration 7

ρ^s_0 intrinsic density for solid phase in reference configuration 7

$\alpha = s, f$ representing the phases, solid or fluid , see equation (2.5) 7

$\boldsymbol{\varphi}$ deformation map , see equation (2.5) 7

$\boldsymbol{X}$ coordinates of a point in reference configuration , see equation (2.5) 7

J Jacobian of the deformation gradient $\boldsymbol{F}$, see equation (2.5) 7

$\boldsymbol{v}$ solid velocity , see equation (2.6) 7

ε^f_v logarithmic compressibility strain for fluid phase , see equation (2.8) 7

ε^s_v logarithmic compressibility strain for solid phase , see equation (2.8) 7

$\boldsymbol{v}^r$ relative velocity 7

$\boldsymbol{v}^d$ Darcy velocity , see equation (2.9) 7

ξ degree of saturation , see equation (2.10) 8

ε^e reversible compaction strain 8

ε^p irreversible wetting compaction 8

$\hat{\rho}^\alpha$ total intrinsic density for each phase , see equation (2.14) 8

$\boldsymbol{h}^\alpha$ local interaction forces for each phase , see equation (2.14) 8

$\boldsymbol{g}$ Gravity constant , see equation (2.14) 8

$\overline{\boldsymbol{t}}$ total traction vector , see equation (2.14) 8

$\overline{\boldsymbol{\sigma}}$ total Cauchy stress , see equation (2.14) 8

$\mathcal{E}$ total internal energy , see equation (2.15) 9

$\mathcal{K}$ total kinetic energy , see equation (2.15) 9

$\frac{D\bullet}{Dt}$ material time derivative 9

e	internal energy , see equation (2.16)	10
$\boldsymbol{l}$	velocity gradient , see equation (2.17)	10
$\boldsymbol{\tau}$	total Kirchhoff stress , see equation (2.33)	13
$\boldsymbol{\tau}^{iso}$	isochoric part of the Kirchhoff stress , see equation (2.33)	13
$\boldsymbol{\tau}^{vol}$	volumetric part of the Kirchhoff stress , see equation (2.33)	13
G	shear modulus , see equation (2.33)	13
K	bulk modulus , see equation (2.33)	13
I_1	first invariant of $\boldsymbol{b}$, see equation (2.33)	13
$\boldsymbol{b}$	left Cauchy-Green deformation tensor , see equation (2.33)	13
E	Young modulus, see equation (2.34)	13
β	packing component, see equation (2.34)	13
p_0	configurational fluid pressure, see equation (2.35)	13
p	fluid pressure, see equation (2.35)	13
μ	viscous resistance , see equation (2.37)	14
ν	fluid viscosity, see equation (2.37)	14
ζ	wetting length, see equation (2.37)	14
r	fiber radius, see equation (2.37)	14
K_{mes}	mesoscopic permeability, see equation (2.37)	14
K_{Ch}	the permeability through the channel, see equation (2.38)	14
$\boldsymbol{K}_{mac}$	anisotropic permeability tensor, see equation (2.38)	14

Part I
Extended Summary

1 Introduction

1.1 Background

Polymer Composite materials have been in use in industry for more than 70 years. Their advantages compare to other materials such as high–performance and lightweight applications have attracted many industries such as aerospace, automotive, infrastructure, sports and marine to explore and increase their usage. There are numerous ways to manufacture fiber reinforced polymer composites ranging from hand lay–up in small series to fully automatic pressing of components to the automotive industry. As it is mentioned by Trochu et. al. [1], five major ways to manufacture structural fiber reinforced composites are presently in use: hand lay–up, autoclave, pultrusion, filament winding and Liquid Composite Molding (LCM). Parnas [2] has compared these processes with respect to manufacturing cost, performance and geometric complexity which are the key parameters to make the right choice between these processes. Over the past few decades researchers and engineers have employed mathematical and numerical tools in order to understand and predict manufacturing of composites. Their aim was to improve the process, increase the product quality and predict the mechanical properties. By increasing the computing power, on one hand, advanced computational methods have been developed to achieve this goal where they have been much more effective and efficient in compare to numerical hand calculation before. On the other hand, it has been raising the issue of the difficulty of developing the models and the numerical procedures that are capable of handling complex problems. In this thesis we are dealing with the development of a continuum thermodynamic framework using the theory of porous media in order to establish a simulation routine for modeling few different composite manufacturing processes.

1.2 Composite materials

Composite materials consist of two or more different materials bonded to each other in order to utilize the properties of each constituent for the structural improvement of the whole assembly. Due to certain properties, composite materials have been a good alternative for many metallic parts, especially in aerospace structures and transport sector. These properties are: high mechanical performance, high specific strength and stiffness, weight reduction resulting in energy saving and good resistance to corrosion. There are three main classifications of composite materials: particle–reinforced, fiber–reinforced and structural composites. In particle–reinforced composites, particle dimensions are approximately the same in all directions and generally particulate phase is harder and stiffer than the matrix. In fiber–reinforced composites, the dispersed phase has the

geometry of a fiber, the mechanical properties mostly depend on the properties of the fibers and applied load is transmitted to the fibers by the matrix phase through the fiber/matrix interface. Structural composites are the combinations of composites and homogeneous materials and the geometrical design of the structural elements affect the mechanical properties of the structure. The most common structural composites are laminated composites and sandwich panels [3].

Fiber Reinforced Plastics (FRP) are now the first choice for fabricating structures where low weight in combination with high strength and stiffness are required. Such materials are sometimes referred to as 'high–performance' composites, and would often be composed of carbon fibers and epoxy resin. Density, stiffness (modulus) and strength are the properties that initially come to mind when thinking of FRP, and these would certainly be the design drivers for materials selection for transport applications such as aircraft, motor vehicles and trains, cf. [4]. Figure 1.1 shows classification of composites based on reinforcing material, showing fiber reinforced composites (fibrous composites) in detail.

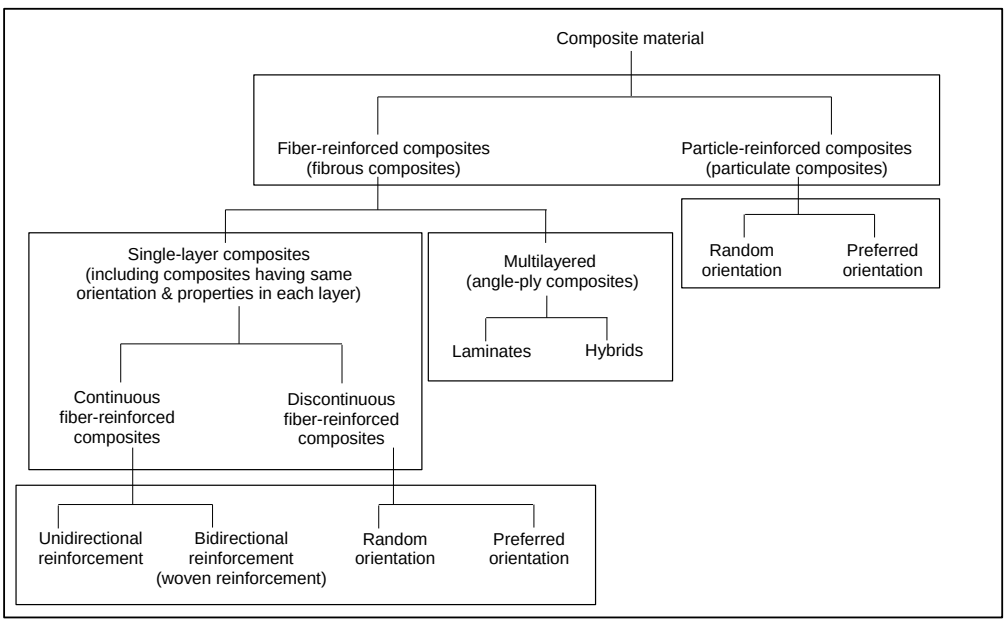

Figure 1.1: Classification of composite materials based on the type of reinforcing material structure [5].

1.3 Composite manufacturing

Manufacturing of composite materials is very different from metals. When producing metal parts, the properties of the virgin material and the finished part are fundamentally

unchanged. In case of composites, the manufacturing process plays a key role. During composite processing, one makes not only the part of the desired shape, but also the material itself with specific properties. In addition, the quality of the composite material and the component fabricated depends on the manufacturing process since it is during the manufacturing process that the matrix material and the fiber reinforcement are combined and consolidated to form the composite. The practice of choosing an appropriate manufacturing method is based on the actual part size and geometry, the unit count, the selected components of the composite, i.e. the reinforcement and the matrix, and the cost.

Previously, the manufacturability of a prototype was usually based on experience and 'trial and error' approaches since numerical procedures had not yet been applied to the development of control systems, which can correlate the main parameter values of the processes with the processing behavior and the final properties of the component [6]. Very little analysis of process physics and back–of–the–envelope calculations were done to approach a prototype development of a composite structure [7]. This way of manufacturing has proved to be expensive and composite industry has come under intense pressure to become cost effective and focus on cost avoidance in prototype development.

Recently, many new manufacturing techniques were invented and introduced and some of them were incrementally improved to increase the yield of manufactured composite parts [7]. As it was mentioned earlier, there are five major ways to manufacture composites. Over the years, by developing new technologies, these manufacturing techniques have also been further developed. For example, Out of Autoclave (OoA) methods are introduced against Autoclave methods in such a way to preserve the high quality of the products but also reduce the manufacturing and tooling costs and time. Another example is Resin Transfer Molding (RTM) from the LCM family where Compression RTM (CRTM) is developed to speed up the cycle time and also overcome the negative aspects of traditional RTM process such as high injection pressure.

Composite manufacturing processes for FRP composites are generally grouped into two general classes: open mold and closed mold. Open mold are those processes in which the part is not inside the mold during the complete duration of the manufacturing process such as pultrusion or filament winding. In closed mold processes, the preform is placed in a mold, the mold is closed, and when it is reopened the part is fabricated. The focus of the current work is on the closed mold processes for continuous–fiber reinforced materials.

1.4 Process modeling of advanced composites

"Advanced (FRP) composites" is referred to those composites that are manufactured by continuous fibers. Analysis have shown that continuous fibers could enhance the mechanical properties by one to two orders of magnitude as compared to short fiber composites [7]. There are several primary steps that are common in manufacturing of advanced (FRP) composites in a closed mold process. First, all advanced composites require a skeleton structure of the fibers or fiber network. Second, this fiber structure must be impregnated by the liquid resin. Finally, the part should be supported by a rigid tool to allow the resin to cure.

The fiber form and the matrix type play a key role in the selection of the manufacturing

process where they influence the manufacturing process physics and modeling significantly. Fibers could be short or long, continuous or discontinuous, aligned or interlaced, etc. The resin could be thermoplastic or thermoset. The geometry of the part to be manufactured also influences the decision and also if the process is carried out in an open mold or a closed mold. These choices influence the physics of mold filling.

Assuming that the process is selected, the process modeling step is generally approached by researchers on two scales, macro and micro scale [8]. The macro–scale is usually the order of the smallest dimension of the composite being manufactured (millimeters). The micro–scale scale is more on the order of a fiber or tow diameter (microns) [7]. What which is interesting to model, from macroscopic perspective, is the overall relationship between the process parameters (such as pressure and flow rate) and global deformation of the composite material that is being formed. Continuum mechanics is a suitable approximation to describe the physics in this scale. From microscopic perspective, one may need to model this physics separately and find an approach to couple it with the macro–scale physics since composite materials are heterogenous materials by definition and macro–level physics cannot capture phenomena that occur on the micro–scale.

In this contribution, we aim for a generic process simulation tool where it is capable of handling the physics in the two different scale mentioned above. For this purpose Theory of Porous Media (TPM) combined with the concept of finite strain hyperelasticity within a well–founded thermodynamical framework has been reiterated. Constitutive relations with respect to sub processes are also formulated. By focusing on nonlinearities (due to large deformation of the preform) of the strongly coupled problem, the developed biphasic continuum mechanical model accounts for the relevant physical properties stemming from the porous microstructure, the moving and interacting incompressible fluid, and the directly coupled intrinsic hyperelasticity of the skeleton material itself. Finally, after the numerical treatment of the governing equations using finite element method, a 2–d problem was simulated to show the efficiency of the numerical implementation.

2 Continuum mechanics of two–phase porous media

2.1 Background

The area of multi–phase materials modeling is a well–established and growing field in the mechanical scientific community. There has been a tremendous development in recent years including the conceptual theoretical core of multi–phase materials modeling, the development of computational methodologies as well as experimental procedures. Examples of the theory applications are civil engineering [9], biomaterial [10] and composites modeling [11] and [12] to name a few. The latter is the focus of the current contribution. Consequently specific related issues concerning modeling of the matter are of interest. Solid–fluid interaction and compressible/incompressible solids/fluids including phenomena like consolidation, compaction, wetting etc. are examples of the modeling challenges. Each of them are well established and formulated separately in isolation from the others.

However, there are instances addressing them in a more coupled fashion, cf. [13] and [14], which is the focus of this thesis for further improvement.

Since the ultimate goal of this research is to develop a simulation tool, the essence of the computational methods is not negligible. Computational mechanics is the discipline concerned with the use of computational methods to study phenomena governed by the principles of mechanics. Here we use Finite Element Analysis (FEA) to simulate the process modeling in composite manufacturing. This is where we use the theory of porous media as the back bone of the modeling. This theory will provide a framework for the modeling of a solid porous material with compressible and incompressible solid and fluid phases. The constitutive relations that have been used here are restricted to hyperelasticity and the ordinary Darcy model describing the interaction between the constituents. The mathematical equations are then formulated which are suitable for digital computation. This step is basically where we derive the weak form of the equations with respect to domain and primary fields. The domain discretization along with primary field identifications are done based on the strongly coupled problem in hand to solve the governing equations of mass and momentum balance along with respective constitutive equations where the Taylor–Hood element has been chosen for the simulation. To solve the discretized equations using finite element analysis an in–house code was developed. Computational procedures associated with the nonlinear response of the coupled two–phase material are also emphasized in our publications. Extensive description and formulation of the matter is exploited in the appended papers with respect to different manufacturing method under consideration.

2.2 The concept of two phase mixture

A system containing a solid–fluid mixture is considered here as a homogenized two phase material. In the problem concerning composite materials we assume a fiber bed as a porous material. The pores are embedded into the solid fiber network and they are either partially filled by liquid resin or contains unfilled void spaces. As a result we have a porous solid which can be completely unsaturated, partially saturated or fully saturated.

It is necessary to adopt a macroscopic view for the description of local quantities such as the stress, the deformation gradient etc. To this end we introduce the Representative Volume Element (RVE) with volume V, with the involved solid–fluid constituents on a sub–scale and the corresponding homogenization on the macro–scale, cf. Figure 2.1. The constituents involved in the process can be assumed to be either compressible or incompressible:

- Compressible solid particles, p, with the volume fraction $\phi^p = V^p/V$, representing the fibers.
- Incompressible liquid constituent, l, with the volume fraction $\phi^l = V^l/V$, representing the resin.
- Voids, v, with volume fraction $\phi^v = V^v/V$, embedded in the fiber plies.
- Compressible gas constituent, g, with volume fraction $\phi^g = V^g/V$, occupying the voids.

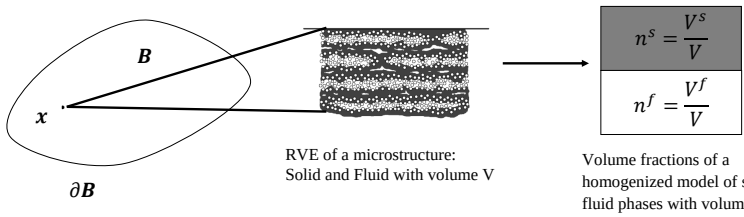

Figure 2.1: The link between micro– and macro–constituents in terms of a representative mixture having volume V.

To ensure that each RVE is occupied by fluid and solid phases we have the saturation constraint as

$$n^s + n^f = 1 \quad with \quad n^s = \phi^p + \phi^v \quad and \quad n^f = \phi^l + \phi^g, \tag{2.1}$$

where n^s and n^f are the macroscopic volume fractions for the solid and fluid phase, respectively. In turn, the solid phase is considered subdivided into particle and void constituents. Likewise, fluid phase is also subdivided into liquid and gas constituents. Identification of the micro–constituents depends on the assumption of having a binary or ternary mixture. In Paper A a ternary mixture is considered where we have incompressible particle and liquid constituents where the voids are occupied by the highly compressible gas. In Paper B and Paper C a binary mixture consists of compressible particles and incompressible liquid occupying the voids is under study. Finally, in Paper D, the mixture is considered to be of compressible particles, incompressible liquid and highly compressible gas constituents.

This representative volume must include enough material for it to be representative of the studied macroscopic behavior, but at the same time, it must be small enough to represent the local dependence of the averaged quantities. Clearly, this view confirms the existence of a "scale" of the elementary volume, which should be sufficiently small as compared to the scale of the intended application.

We may thus formulate the volume V of the RVE in terms of the volume fractions as

$$V = V^s + V^f = \int_{\mathcal{B}^s} dv + \int_{\mathcal{B}^f} dv = \int_{\mathcal{B}} n^s dv + \int_{\mathcal{B}} n^f dv = \int_{\mathcal{B}} (n^s + n^f) dv = \int_{\mathcal{B}} dv. \tag{2.2}$$

The application of the principle of mass equivalence, between the micro– and the macroscopic mass, to the RVE with volume V we have

$$\begin{aligned} \mathcal{M} = \int_{\mathcal{B}^s} \rho^s_{mic} dv + \int_{\mathcal{B}^f} \rho^f_{mic} dv = \int_{\mathcal{B}} n^s \rho^s_{mic} dv + \int_{\mathcal{B}} n^f \rho^f_{mic} dv = \\ \int_{\mathcal{B}} (n^s \rho^s_{mic} + n^f \rho^f_{mic}) dv = \int_{\mathcal{B}} (n^s \rho^s + n^f \rho^f) dv \overset{\text{P.S.S}}{=} (n^s \rho^s + n^f \rho^f) V, \end{aligned} \tag{2.3}$$

where the macroscopic intrinsic densities are associated with each constituent, as denoted ρ^s and ρ^f, are introduced. According to the Principle of Scale Separation (P.S.S.), i.e. that the involved macroscopic quantities can be considered constant across the RVE, we

could state the relationship between the microscopic and the macroscopic fields as in the last equality in (2.3). Now we can obtain the averages

$$\begin{aligned} n^s\rho^s &= \frac{1}{V}\int_{\mathcal{B}^s}\rho^s_{mic}dv \Rightarrow \rho^s = \frac{1}{V^s}\int_{\mathcal{B}^s}\rho^s_{mic}dv, \\ n^f\rho^f &= \frac{1}{V}\int_{\mathcal{B}^f}\rho^f_{mic}dv \Rightarrow \rho^f = \frac{1}{V^f}\int_{\mathcal{B}^f}\rho^f_{mic}dv. \end{aligned} \tag{2.4}$$

It may be noted that the intrinsic densities relate to the issue of compressibility (or incompressibility) of the phases. For example, in the case of an incompressible porous mixture, the intrinsic densities are stationary with respect to their reference configurations, i.e. $\rho^s = \rho^s_0$, $\rho^f = \rho^f_0$.

2.3 Conservation of mass

The basic idea behind the formulation of mass conservation is that the mass of the constituents is conserved during deformation, i.e.

$$m^\alpha_0[\boldsymbol{X}^\alpha] = m^\alpha[\boldsymbol{\varphi}[\boldsymbol{X}^\alpha]] \Leftrightarrow \rho^\alpha_0 dV = \rho^\alpha J dV, \tag{2.5}$$

where it was used that $m^\alpha = \rho^\alpha dv$, $\boldsymbol{\varphi}[\boldsymbol{X}^\alpha]$ are deformation maps and $J = det[\boldsymbol{F}]$ is the Jacobian of the deformation gradient for α phases representing solid, s, and fluid, f, phases respectively. Considering the situation of the two phase mixture we can formulate the mass conservation of the two–phase material, cf. (2.3), as

$$\dot{M}^s + \dot{M}^f + J\boldsymbol{\nabla}\cdot(n^f\rho^f\boldsymbol{v}), \tag{2.6}$$

where the solid and fluid contents may be expanded in terms of the volume fractions as

$$\begin{aligned} M^s = Jn^s\rho^s \Rightarrow \dot{M}^s &= J\rho^s\left(\dot{n}^s + n^s\boldsymbol{\nabla}\cdot\boldsymbol{v} + n^s\frac{\dot{\rho}^s}{\rho^s}\right), \\ M^f = Jn^f\rho^f \Rightarrow \dot{M}^f &= J\rho^f\left(\dot{n}^f + n^f\boldsymbol{\nabla}\cdot\boldsymbol{v} + n^f\frac{\dot{\rho}^f}{\rho^f}\right). \end{aligned} \tag{2.7}$$

In the context of this thesis, to be able to model the involved physics during the process modeling of composite materials, we have introduced the logarithmic compressibility strains ε^s_v for the solid phase densification and ε^f_v for the fluid phase densification expressed in terms of the intrinsic densities ρ^s and ρ^f as

$$\begin{aligned} \varepsilon^s_v &= -\log[\frac{\rho^s}{\rho^s_0}] \Rightarrow \dot{\varepsilon}^s_v = -\frac{\dot{\rho}^s}{\rho^s} \Rightarrow \frac{\dot{\rho}^s}{\rho^s} = -\dot{\varepsilon}^s_v, \\ \varepsilon^f_v &= -\log[\frac{\rho^f}{\rho^f_0}] \Rightarrow \dot{\varepsilon}^f_v = -\frac{\dot{\rho}^f}{\rho^f} \Rightarrow \frac{\dot{\rho}^f}{\rho^f} = -\dot{\varepsilon}^f_v. \end{aligned} \tag{2.8}$$

Now, the mass balance relation in equation (2.6), using the solid and fluid contents in equation (2.7) and introducing the Darcy velocity as $\boldsymbol{v}^d = n^f\boldsymbol{v}^r$, become

$$\boldsymbol{\nabla}\cdot\boldsymbol{v} - n^s\dot{\varepsilon}^s_v - n^f\dot{\varepsilon}^f_v = -\frac{1}{\rho^f}\boldsymbol{\nabla}\cdot(\rho^f\boldsymbol{v}^d), \tag{2.9}$$

where saturation constraint in equation (2.1) and its rate have been used.

In Paper A, the conservation of mass presented there was formulated in such a way to present only the compressibility of the fluid phase, $\rho^f = \rho^f[\boldsymbol{\varphi}[\boldsymbol{X}], t]$, while solid phase was considered incompressible. The fluid density considered compressible due to gas density, $\rho^g = \rho^g[p]$, in view of the definition of the degree of saturation, $\rho^f = \xi\rho^l + (1-\xi)\rho^g$, where the total mass balance relation became

$$\boldsymbol{\nabla}\cdot\boldsymbol{v} - n^f\dot{\varepsilon}^f_v = -\frac{1}{\rho^f}\boldsymbol{\nabla}\cdot\left(\frac{\rho^f}{\xi}\boldsymbol{v}^d\right), \quad \text{with } \dot{\varepsilon}^f_v = -\frac{\dot{\rho}^f}{\rho^f}, \tag{2.10}$$

where a governing equation for saturation degree evolution was also established in order to monitor the moving free surface at the flow front during resin infusion where the formulation was traversing into incompressibility with increasing partial saturation as

$$n^f\dot{\xi} + \frac{\dot{J}}{J}\xi + \boldsymbol{\nabla}\cdot\boldsymbol{v}^d = 0, \tag{2.11}$$

where it may be noted that there are two sources governing $\dot{\xi}$, namely, volumetric solid deformation and the liquid divergence term $\boldsymbol{\nabla}\cdot\boldsymbol{v}^d$.

In Paper B and Paper C, where we tackled the press forming manufacturing processes, the solid phase compressibility was the key feature of the formulation and the aim was to present the total compaction of the solid phase with the reversible compaction strain and irreversible wetting compaction as $\varepsilon^s_v = \varepsilon^e + \varepsilon^p$. In that sense the mass balance in equation (2.9) was modified to have

$$\boldsymbol{\nabla}\cdot\boldsymbol{v} - n^s\dot{\varepsilon}^s_v = -\boldsymbol{\nabla}\cdot\boldsymbol{v}^d, \quad \text{with } \dot{\varepsilon}^s_v = -\frac{\dot{\rho}^s}{\rho^s}. \tag{2.12}$$

Finally, in Paper D, we made the choice for the use of compressibility for the both phases and we used equation (2.9) in full format. Here we aimed to model sub–processes in micro and macro scale at the same time. At macro scale the fluid compressibility, in the same way as in Paper A, will be deriving the governing equation for saturation degree evaluation. There is a difference here, however. The solid phase compressibility representing micro infiltration and compaction will also affect this governing equation where we have

$$n^f\dot{\xi} + \left(\frac{\dot{J}}{J} - (1-n^f)\dot{\varepsilon}^s_v\right)\xi + \boldsymbol{\nabla}\cdot\boldsymbol{v}^d = 0. \tag{2.13}$$

2.4 Balance of momentum

The linear momentum balance of the solid and fluid, occupying the region $\mathcal{B}$ and $\mathcal{B}^f_0$ respectively, as in Figure 2.2, is obtained in the spatial format for the mixture as

$$\begin{aligned} \boldsymbol{\sigma}^s\cdot\boldsymbol{\nabla} + \hat{\rho}^s\boldsymbol{g} + \boldsymbol{h}^s &= 0, \\ \boldsymbol{\sigma}^f\cdot\boldsymbol{\nabla} + \hat{\rho}^f\boldsymbol{g} + \boldsymbol{h}^f &= 0, \end{aligned} \tag{2.14}$$

where $\boldsymbol{\sigma}^s$ and $\boldsymbol{\sigma}^f$ are the Cauchy stresses for each phase from the resulting traction vector $\overline{\boldsymbol{t}} = (\boldsymbol{\sigma}^s + \boldsymbol{\sigma}^f) \cdot \boldsymbol{n}$ acting along the external boundary $\partial\mathcal{B}$, $\boldsymbol{n}$ is the outward normal vector, $\boldsymbol{g}$ is the gravity and $\boldsymbol{h}^\alpha$ are the local interaction forces for each phase. The total Cauchy stress $\overline{\boldsymbol{\sigma}} = \boldsymbol{\sigma}^s + \boldsymbol{\sigma}^f$ is also related to the effective (constitutive) stress $\boldsymbol{\sigma}$ and the fluid pressure p via the Terzaghi effective stress principle, i.e. $\overline{\boldsymbol{\sigma}} = \boldsymbol{\sigma} - p\mathbf{1}$.

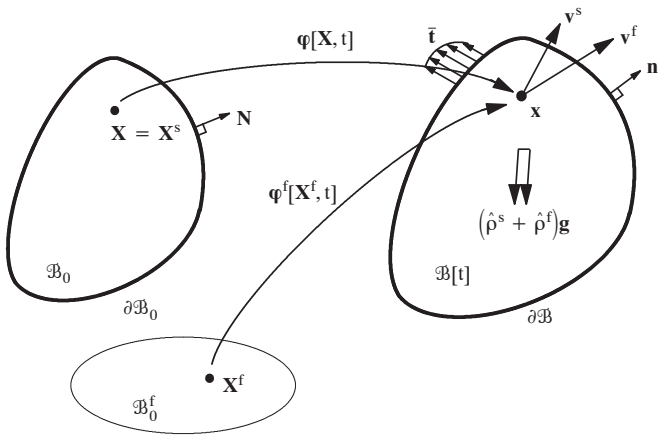

Figure 2.2: Solid and fluid in equilibrium with respect to reference and deformed configurations.

In addition to linear momentum balance, angular momentum balance should be considered as well. However, in the concept of composite manufacturing, we have assumed quasi static behavior for the mixture. In that sense we can neglect the angular momentum balance.

2.5 Balance of energy

To establish a continuum thermodynamical framework for the binary mixture in the concept of composite manufacturing the first law od thermodynamic needs to be fulfilled. If we establish the principle of energy conservation written as the balance relation applied to the mixture of solid and fluid phases, we will have

$$\frac{D\mathcal{E}}{Dt} + \frac{D\mathcal{K}}{Dt} = W + Q, \tag{2.15}$$

where $\mathcal{E} = \mathcal{E}^s + \mathcal{E}^f$ is the total internal energy and $\mathcal{K} = \mathcal{K}^s + \mathcal{K}^f$ is the total kinetic energy of the mixture solid and the total material velocity with respect to the mixture material is defined as ${}^{D}\bullet/_{Dt} = {}^{D^s}\bullet/_{Dt} + {}^{D^f}\bullet/_{Dt}$. Moreover, W is the mechanical work rate of the solid and Q is the heat supply to the solid. We are assuming an isothermal and quasi–static situation which will result in ${}^{D\mathcal{K}}/_{Dt} = Q = 0$. The contribution of the internal energy

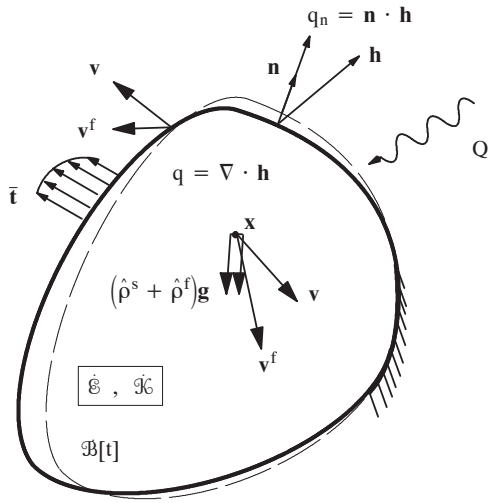

Figure 2.3: Quantities involved in the formulation of the principle of energy conservation.

from individual phases is then follow as

$$\frac{D\mathcal{E}}{Dt} = \int_{\mathcal{B}} (\hat{\rho}^s \dot{e}^s + \hat{\rho}^f \dot{e}^f + \hat{\rho}^f (\boldsymbol{\nabla} e^f) \cdot \boldsymbol{v}^r) dv = \int_{\mathcal{B}} (\dot{\hat{e}} + \hat{\rho}^f (\boldsymbol{\nabla} e^f) \cdot \boldsymbol{v}^r) dv, \tag{2.16}$$

where the rate of the fluid content relation presented in equation (2.7) is used and the relative velocity, $\boldsymbol{v}^r = \boldsymbol{v} - \boldsymbol{v}^f$, is introduced. We also introduced the (solid) material change of internal energy of the mixture as $\dot{\hat{e}} = \hat{\rho}^s \dot{e}^s + \hat{\rho}^f \dot{e}^f$.

In view of Figure 2.3 we formulate the mechanical work rate produced by the gravity forced in $\mathcal{B}$ and the forces acting on the external boundary Γ as

$$\begin{aligned} W &= \int_{\mathcal{B}} (\hat{\rho}^s \boldsymbol{g} \cdot \boldsymbol{v} + \hat{\rho}^f \boldsymbol{g} \cdot \boldsymbol{v}^f) dv + \int_{\mathcal{B}} (\boldsymbol{v} \cdot (\boldsymbol{\sigma}^s \cdot \boldsymbol{n}) + \boldsymbol{v}^f \cdot (\boldsymbol{\sigma}^f \cdot \boldsymbol{n})) d\Gamma = \\ &= \{...\} = \int_{\mathcal{B}} (\boldsymbol{\sigma}^s : \boldsymbol{l} + \boldsymbol{\sigma}^f : \boldsymbol{l}^f - \boldsymbol{h}^f \cdot \boldsymbol{v}^r) dv, \end{aligned} \tag{2.17}$$

where the Divergence theorem and the momentum balance relations in equation (2.14) along with some additional derivations has been used. Thus, the localized format of the energy equation will read as

$$\dot{\hat{e}} = \boldsymbol{\sigma}^s : \boldsymbol{l} + \boldsymbol{\sigma}^f : \boldsymbol{l}^f - \boldsymbol{h}^f \cdot \boldsymbol{v}^r - \hat{\rho}^f (\boldsymbol{\nabla} e^f) \cdot \boldsymbol{v}^r. \tag{2.18}$$

At the end we need to represent the fluid phase term $\boldsymbol{\sigma}^f : \boldsymbol{l}^f$ in equation (2.18) to the motion of the solid phase. So we can rewrite this term as

$$\begin{aligned} \boldsymbol{\sigma}^f : \boldsymbol{l}^f &= \boldsymbol{\sigma}^f : (\boldsymbol{l} + \boldsymbol{l}^r) = \{...\} = \boldsymbol{\sigma}^f : \boldsymbol{l} + \boldsymbol{\nabla} \cdot (\boldsymbol{v}^r \cdot \boldsymbol{\sigma}^f) - \boldsymbol{v}^r \cdot \boldsymbol{\nabla} \cdot \sigma^f = \\ &= \boldsymbol{\sigma}^f : \boldsymbol{l} + \boldsymbol{\nabla} \cdot (\boldsymbol{v}^r \cdot \boldsymbol{\sigma}^f) + \boldsymbol{v}^r \cdot \left(\boldsymbol{h}^f + \hat{\rho}^f \boldsymbol{g} \right), \end{aligned} \tag{2.19}$$

where we used equilibrium for the fluid phase presented in equation (2.14b). Hence, the relation (2.18) is re–established as

$$\dot{\hat{e}} = (\boldsymbol{\sigma}^s + \boldsymbol{\sigma}^f) : \boldsymbol{l} + \boldsymbol{\nabla} \cdot (\boldsymbol{v}^r \cdot \boldsymbol{\sigma}^f) + \hat{\rho}^f \boldsymbol{v}^r \cdot (\boldsymbol{g} - \boldsymbol{\nabla} e^f). \tag{2.20}$$

Assuming a non–viscous fluid, the fluid stress may be represented as $\boldsymbol{\sigma}^f = -n^f p \mathbf{1}$. In view of this assumption we can formulate the term $\boldsymbol{\nabla} \cdot (\boldsymbol{v}^r \cdot \boldsymbol{\sigma}^f)$ of equation (2.20) as

$$\boldsymbol{\nabla} \cdot (\boldsymbol{v}^r \cdot \boldsymbol{\sigma}^f) = -\boldsymbol{\nabla} \left(\hat{\rho}^f \frac{p}{\rho^f} \boldsymbol{v}^r \right) = -\frac{p}{\rho^f} \boldsymbol{\nabla} \cdot (\rho^f \boldsymbol{v}^d) - \rho^f \boldsymbol{v}^d \boldsymbol{\nabla} \cdot \left(\frac{p}{\rho^f} \right), \tag{2.21}$$

where introducing the Darcian velocity $\boldsymbol{v}^d = n^f \boldsymbol{v}^r$ is considered. Now, combination of the term $-(p \boldsymbol{\nabla} \cdot (\rho^f \boldsymbol{v}^d))/\rho^f$ with the balance of mass of the mixture material in equation (2.9) we obtain

$$-\frac{p}{\rho^f} \boldsymbol{\nabla} \cdot (\rho^f \boldsymbol{v}^d) = p \boldsymbol{\nabla} \cdot \boldsymbol{v} - n^s p \dot{\varepsilon}_v^s - n^f p \dot{\varepsilon}_v^f, \tag{2.22}$$

where replacing (2.22) in equation (2.21) and consequently in equation (2.20) leads to

$$\dot{\hat{e}} = \boldsymbol{\sigma} : \boldsymbol{l} - n^s p \dot{\varepsilon}_v^s - n^f p \dot{\varepsilon}_v^f + \rho^f \boldsymbol{v}^d \cdot \left(\boldsymbol{g} - \boldsymbol{\nabla} e^f - \boldsymbol{\nabla} \cdot \left(\frac{p}{\rho^f} \right) \right) \tag{2.23}$$

where the effective stress $\boldsymbol{\sigma} = \overline{\boldsymbol{\sigma}} + p\mathbf{1}$, of Terzaghi is defined and used during the manipulations.

2.6 Entropy inequality

For establishing constitutive relations in the thermodynamical framework we are considering the second law of thermodynamics formulated in terms of the total entropy $\mathcal{S}$ for the mixture written as

$$\mathcal{S} = \int_{\mathcal{B}} (\hat{\rho}^s s^s + \hat{\rho}^f s^f) dv, \tag{2.24}$$

where s^s and s^f are the local entropies per unit mass of the solid and fluid phases, respectively. We assumed that the temperature is constant, i.e. it is stationary, and it is common for both phases, i.e. we have that $\theta = \theta^s = \theta^f$.

The second law of thermodynamics (simply the entropy inequality) can be stated as

$$\frac{D\mathcal{S}}{Dt} - Q_\theta \geq 0, \tag{2.25}$$

where ${}^{D\mathcal{S}}/_{Dt}$ is the total time derivative of our two–phase porous material. Moreover, Q_θ, the net heat thermal supply per temperature unit, is considered zero for the isothermal case that we are dealing with.

The total material derivative of the total entropy is obtained, with consideration of the balance of mass stated in equation (2.7), as

$$\begin{aligned} &\frac{D\mathcal{S}}{Dt} = \int_{\mathcal{B}} \left(\hat{\rho}^s \frac{D^s s^s}{Dt} + \hat{\rho}^f \frac{D^f s^f}{Dt} \right) dv = \{...\} = \\ &= \int_{\mathcal{B}} (\hat{\rho}^s \dot{s}^s + \hat{\rho}^f \dot{s}^f + \hat{\rho}^f (\boldsymbol{\nabla} s^f) \cdot \boldsymbol{v}^r) dv = \int_{\mathcal{B}} (\dot{\hat{s}} + \hat{\rho}^f (\boldsymbol{\nabla} s^f) \cdot \boldsymbol{v}^r) dv, \end{aligned} \tag{2.26}$$

where $\dot{\hat{s}} = \hat{\rho}^s \dot{s}^s + \hat{\rho}^f \dot{s}^f$ is the saturated entropy change. In the localized format, the entropy inequality can be written, in view of equation (2.25) as

$$D^{mech} = \dot{\hat{s}} + \hat{\rho}^f (\boldsymbol{\nabla} s^f) \cdot \boldsymbol{v}^r \geq 0, \tag{2.27}$$

where we require that the mechanical portion of the inequality to be satisfied independently.

We can develop D^{mech} further using the Legendre transformation. Legendre Transformation is introduced to relate generically the internal energy e, the free energy ψ and the entropy s to each other via

$$e[\boldsymbol{A}, \theta] = \psi[\boldsymbol{A}, \theta] + s\theta, \tag{2.28}$$

where ψ is the Helmholtz free energy representing the stored reversible energy as a function of the internal variables $\boldsymbol{A}$.

Now using the relation (2.28) we can rewrite equation (2.27) as

$$D^{mech} = \dot{\hat{e}} - \dot{\hat{\psi}} + \hat{\rho}^f (\boldsymbol{\nabla}(e^f - \psi^f) - s^f \underbrace{\boldsymbol{\nabla}\theta}_{=0}) \cdot \boldsymbol{v}^r \geq 0, \tag{2.29}$$

where it was used that $\theta \boldsymbol{\nabla} s^f = \boldsymbol{\nabla}(\theta s^f) - s^f \boldsymbol{\nabla}\theta$. Now combination with energy equation in (2.23) yields

$$D^{mech} = \boldsymbol{\sigma} : \boldsymbol{l} - n^s p \dot{\varepsilon}_v^s - \hat{\rho}^s \dot{\psi}^s - n^f p \dot{\varepsilon}_v^f - \hat{\rho}^f \dot{\psi}^f + \rho^f \boldsymbol{v}^d \cdot \left(\boldsymbol{g} - \boldsymbol{\nabla}\psi^f - \boldsymbol{\nabla} \cdot \left(\frac{p}{\rho^f} \right) \right) \geq 0, \tag{2.30}$$

whereby the final result in fact may be interpreted in terms of a number of independent phenomenological mechanisms of the mixture material as

$$\begin{aligned}
&D^{mech} = D^s + D^{nvf} + D^i \geq 0, \text{ where} \\
&D^s = \boldsymbol{\sigma} : \boldsymbol{l} - n^s p \dot{\varepsilon}_v^s - \hat{\rho}^s \dot{\psi}^s \geq 0, \\
&D^{nvf} = -n^f p \dot{\varepsilon}_v^f - \hat{\rho}^f \dot{\psi}^f = 0, \\
&D^i = \rho^f \boldsymbol{v}^d \cdot \left(\boldsymbol{g} - \boldsymbol{\nabla}\psi^f - \boldsymbol{\nabla} \cdot \left(\frac{p}{\rho^f} \right) \right) = -\boldsymbol{h}_e^f \cdot \boldsymbol{v}^d \geq 0,
\end{aligned} \tag{2.31}$$

where $D^s \geq 0$ is the dissipation produced by the (homogenized) solid phase material considered as an independent process of the mixture. The term D^{nvf} represents dissipation in the non–viscous stress response of the fluid. It is assumed that this dissipation can be neglected, i.e. $D^{nvf} := 0$. The term $D^i \geq 0$ represents dissipation induced by drag–interaction between the phases. However, in formulation of $\boldsymbol{h}_e^f$, for later use where we are developing the constitutive equation for solid and fluid interaction, it is of interest to use the constitutive relation resulted from D^{nvf} for pressure as $p = -\rho^f \partial\psi^f / \partial\varepsilon_v^f$ and simplify the term $\boldsymbol{h}_e^f$. In this view we have

$$-\boldsymbol{\nabla}\left(\frac{p}{\rho^f} \right) - \boldsymbol{\nabla}\psi^f = -\frac{1}{\rho^f}\boldsymbol{\nabla} + \left(p \frac{1}{(\rho^f)^2} - \frac{\partial\psi^f}{\partial\varepsilon_v^f} \frac{\partial\varepsilon_v^f}{\partial\rho^f} \right) \boldsymbol{\nabla}\rho^f = -\frac{1}{\rho^f}\boldsymbol{\nabla} p. \tag{2.32}$$

leading to $\boldsymbol{h}_e^f = \boldsymbol{g} - \boldsymbol{\nabla} p$.

The dissipative mechanisms developed in this section are the fundamental thinking behind the development of the next section where we formulate the constitutive relations with respect to the concept of the two phase material of the structure under study.

2.7 Constitutive relations

In this section the constitutive equations in respect to the formulated mass and momentum balance in the content of the two phase mixture will be formulated. We have assumed hyper elasticity of the effective stress response and also that the material will behave like a Neo–Hooke material.

Effective fiber bed response

The stress state in the current computational domain, $\boldsymbol{\tau} = J\boldsymbol{\sigma}$, is expressed based on the Neo–Hooke model and is split to isochoric and volumetric response for an isotropic hyperelastic model as

$$\boldsymbol{\tau} = \boldsymbol{\tau}^{iso} + \boldsymbol{\tau}^{vol} \Rightarrow \left\{ \begin{array}{l} \boldsymbol{\tau}^{iso} = GJ^{-2/3}(\boldsymbol{b} - \frac{I_1}{3}\mathbf{1}) \\ \boldsymbol{\tau}^{vol} = KJ(J-1)\mathbf{1} \end{array} \right. , \tag{2.33}$$

where $I_1 = \mathbf{1} : \boldsymbol{b}$, $\boldsymbol{b} = \boldsymbol{F} \cdot \boldsymbol{F}^t$, $\boldsymbol{F} = \partial \boldsymbol{x}/\partial \boldsymbol{X}$ is the deformation gradient and $J = det(\boldsymbol{F})$. The parameters involved in this expression are G and K are the shear and bulk modulus of the macroscopic fibre bed response. This is the assumption that has been made in Paper A for the fiber bed effective response.

However, in Paper B, Paper C and Paper D, we modified the response model by introducing the packing law to the volumetric deformation of the fiber bed. In that sense the volumetric stress response, $\boldsymbol{\tau}^{vol}$, will be formulated differently using that the argument of packing is the fiber volume fraction $\phi^p = \phi_0^p/J$ where ϕ_0^p is the initial volume fraction of particles,

$$\boldsymbol{\tau} = \boldsymbol{\tau}^{iso} + \boldsymbol{\tau}^{vol} \Rightarrow \left\{ \begin{array}{l} \boldsymbol{\tau}^{iso} = GJ^{-2/3}(\boldsymbol{b} - \frac{I_1}{3}\mathbf{1}) \\ \boldsymbol{\tau}^{vol} = -k^s EJ \left((\frac{\phi_0^p}{J})^\beta - (\phi_0^p)^\beta \right) \end{array} \right. . \tag{2.34}$$

Solid compaction and micro–infiltration

The solid phase was considered to be incompressible during the modeling in contribution of Paper A, i.e. $\rho^s = \rho_0^s$. However, in Paper B, Paper C and Paper D, the compressibility of the solid phase was a key feature of the formulations. In that sense the semi–empirical elastic fiber packing law proposed by Toll [15] was directly generalized to the compressive response of the non–saturated region of a fiber bed consisting of voids and dry particles as $p + p_0 = kE\phi^\alpha$, where p_0 is the configurational fluid pressure, cf. to Figure 2.4. Based on the assumptions we made, cf. Rouhi et al. [12], pressure p and the rate formulated compliance form of p, meaning the compaction strain ε_v^s, are formulated as

$$p = p_0 \left(a^\alpha - 1\right) \text{ with } a = \frac{\varphi}{\varphi_0} = \frac{e^{\varepsilon^p} - \phi_0}{e^{\varepsilon_v^s}(1-\phi_0) - \phi_0(1 - e^{\varepsilon^p})}, \tag{2.35}$$

$$e^{\varepsilon_v^s} = -\frac{e^{\varepsilon^p} - \phi_0}{\alpha(p+p_0)(1-\phi_0)} \left(\frac{p+p_0}{p_0} \right)^{-1/\alpha} \dot{p} - e^{\varepsilon^p} \frac{\left(\left(\frac{p+p_0}{p_0} \right)^{-1/\alpha} - \phi_0 \right)}{1-\phi_0} \frac{p}{\mu}, \tag{2.36}$$

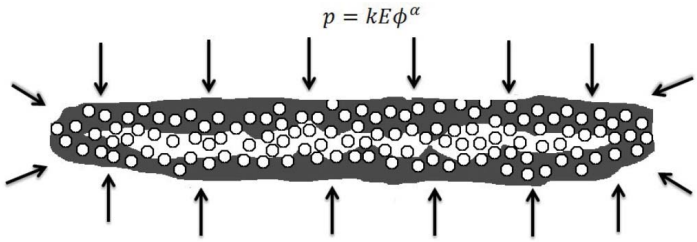

Figure 2.4: Hyperelastic packing of fiber content ϕ in dry region induced by fluid pressure of representative fiber ply in the fiber bed at a fixed value of the micro infiltration ξ.

where ϕ_0 is the initial dry fiber volume content. We can also identify the relation for the irreversible wetting compaction rate as $\dot{\varepsilon}^p = -p/\mu$. The parameter μ then represents the viscous resistance for penetration of liquid into the bulk fibers, which is defined as

$$\mu = \frac{\nu(1-\phi_0)\zeta^2}{K_{mes}}, \qquad with \qquad K_{mes} = \frac{16r^2}{9\pi\sqrt{2}}\left[\sqrt{\frac{\pi}{2\phi\sqrt{3}}} - 1\right]^{5/2}, \tag{2.37}$$

where ν is the fluid viscosity and ζ is the wetting length. The mesoscopic permeability K_{mes} for fiber plies, which is the permeability through the fiber bed, is calculated based on the Gebart equation, cf. [16], for hexagonal fiber packing where r is the fiber radius. In this study the fiber content is considered to be constant where we have used $\phi = \phi_0$ in equation (2.37).

Darcian solid–fluid interactions

Another contribution to the constitutive behavior of the process represents dissipation induced by drag interaction between the phases. To accommodate this dissipation, the effective drag force $\boldsymbol{h}_e^f = \nabla p$ (or hydraulic gradient with negative sign and neglecting gravity $\boldsymbol{g}$) is chosen to ensure positive dissipation via Darcy's law

$$\boldsymbol{v}^d = -\frac{1}{\nu}(\boldsymbol{K}_{mac}) \cdot \boldsymbol{h}_e^f = -\frac{1}{\nu}\left((K_{mes}(1-\phi^l) + K_{Ch}\phi^l)(1-\boldsymbol{M}) + K_{mes}\boldsymbol{M}\right) \cdot \nabla p, \tag{2.38}$$

where $\boldsymbol{K}_{mac}$ is the anisotropic permeability tensor, K_{mes} is the permeability through the fiber, K_{Ch} is the permeability through the channel, cf. Figure 2.5, ϕ^l is liquid volume fraction and $\boldsymbol{M} = \boldsymbol{t} \otimes \boldsymbol{t}$ is the structure tensor related to the director field $\boldsymbol{t}$. For details regarding macroscopic permeability model refer to the Rouhi et al. [12]. This is the general anisotropic deformation–dependent case of the permeability model. It is possible to simplify the model for, for example, deformation–dependent Kozen–Carman model where the effect of the solid deformation in the micro scale is not considered.

Compressible liquid–gas response

In order to assess the pressure dependence in the fluid density $\rho^f = \xi^f\rho^l + (1-\xi^f)\rho^g$, it is assumed that the same pressure prevails in the liquid and gas constituents and that

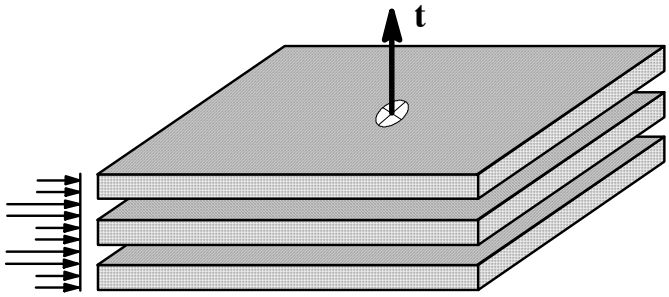

Figure 2.5: Flow channel with orientation $\boldsymbol{t}$ and fiber bed stacks

the highly compressible gas constituent is pressure dependent in the sprit of the ideal gas law, i.e. $\rho^g = k^g p$, where typically the gas–compliance k^g is determined by $k^g = m^g/R\theta$, where m^g is the molecular mass of the gas, R is the universal gas constant and θ is the absolute temperature. It should be noted that the rate behaviour of the fluid density may be characterized in terms of the compression modulus of the liquid–gas mixture defined as

$$\dot{\rho}^f = \frac{1}{K^f}\dot{p} + (\rho^l - \rho^g)\dot{\xi}^f \qquad with \qquad K^f = \frac{1}{(1-\xi^f)k^g}. \tag{2.39}$$

Indeed, the value of K^f increases for increased saturation and decreased gas–compliance k^g. For continued saturation towards $\xi^f = 1$, we obtain that $K^f \to \infty$ and $\xi^f \to 0$ leading to fluid incompressibility, i.e. $\rho^f \to \rho^l$.

2.8 Numerical implementations

In order to numerically solve the established framework, the finite element representation of the involved primary fields and governing equations of momentum and mass balances are considered. To be able to formulate the respective weak form of the governing equations we identify the primary variables for the coupled set of equations in (2.9) and (2.14) where a finite element subdivision of the region D into elements D_e, e=1,..., NEL is made. It is assumed that each element has the interpolation

$$\boldsymbol{\varphi} = \sum_{I=1}^{\mathrm{NODE}_u} N^I[\boldsymbol{X}]\boldsymbol{\varphi}^I = \hat{\boldsymbol{N}}^e_u\hat{\boldsymbol{\varphi}}_e \Rightarrow \boldsymbol{w} = \delta\boldsymbol{\varphi} = \sum_{I=1}^{\mathrm{NODE}} N^I[\boldsymbol{X}]\boldsymbol{w}^I = \hat{\boldsymbol{N}}^e_u\hat{\boldsymbol{w}}_e, \tag{2.40}$$

where $\hat{\boldsymbol{N}}^e_u$ contains the element shape functions and $\hat{\boldsymbol{\varphi}}_e$ is the vector element nodal placements. We then obtain the spatial velocity gradient as

$$\boldsymbol{l} = \sum_{I=1}^{\mathrm{NODE}} \boldsymbol{v}^I \otimes \boldsymbol{g}^I \ , \quad \nabla\cdot\boldsymbol{v} = \sum_{I=1}^{\mathrm{NODE}} \boldsymbol{v}^I \cdot \boldsymbol{g}^I \text{ with } \boldsymbol{g}^I = \boldsymbol{G}^I\cdot\boldsymbol{F}^{-1} \text{ and } \boldsymbol{G}^I = \frac{\partial N^I}{\partial \boldsymbol{X}}, \tag{2.41}$$

where $N^I[\boldsymbol{X}]$ are the element interpolation functions and $\boldsymbol{\varphi}^I$ are the corresponding element nodal placements.

Likewise, the fluid pressure field is approximated, i.e. it is assumed that each element has the interpolation

$$p = \sum_{I=1}^{\text{NODE}_p} N^I[\boldsymbol{X}] p^I = \hat{\boldsymbol{N}}_p^e \hat{\boldsymbol{p}}_e \Rightarrow \eta = \sum_{I=1}^{\text{NODE}_p} N^I[\boldsymbol{X}] \eta^I = \hat{\boldsymbol{N}}_p^e \hat{\boldsymbol{\eta}}_e, \tag{2.42}$$

where e.g. $\hat{\boldsymbol{p}}_{\boldsymbol{e}}$ is the vector nodal pressures. We thus obtain the pressure gradient as $\nabla p = \boldsymbol{B}_p \hat{\boldsymbol{p}}_e$, where $\boldsymbol{B}_p$ is the consequent pressure gradient interpolation matrix. The rate of pressure is relative to the solid reference configuration and is defined by

$$q = \dot{p} = \sum_{I=1}^{\text{NODE}_p} N^I[\boldsymbol{X}] q^I = \hat{\boldsymbol{N}}_p^e \hat{\boldsymbol{q}}_e, \tag{2.43}$$

whereby the integrated nodal displacements $\hat{\boldsymbol{u}}$ and nodal pressures $\hat{\boldsymbol{p}}$ may be assessed as

$$\hat{\boldsymbol{u}} = {}^n\hat{\boldsymbol{u}} + \Delta t \hat{\boldsymbol{v}} \ , \quad \hat{\boldsymbol{p}} = {}^n\hat{\boldsymbol{p}} + \Delta t \hat{\boldsymbol{q}}. \tag{2.44}$$

Then the weak form read as

$$\int_{B_0} J \left(\boldsymbol{\sigma} - p^f \mathbf{1} \right) : \boldsymbol{l}[\boldsymbol{w}] dV = \int_{\Gamma_0} \boldsymbol{w} \cdot \bar{\boldsymbol{t}}_1 d\Gamma_0 + \int_{B_0} \hat{\rho} \boldsymbol{w} \cdot \boldsymbol{g} dV \quad \forall \boldsymbol{w} \in P, \tag{2.45}$$

$$\begin{aligned} &\int_{B_0} \eta \dot{J} dV - \int_{B_0} \eta n_0^s e^{\varepsilon_v^s} \dot{\varepsilon}_v^s dV - \int_{B_0} \eta J n^f \dot{\varepsilon}^f dV - \\ &\int_{B_0} J \frac{1}{\xi} (\nabla \eta) \cdot \boldsymbol{v}^d dV = - \int_{\Gamma_0} \eta Q d\Gamma_0 \quad \forall \eta \in S, \end{aligned} \tag{2.46}$$

where it was used that $\dot{J} = \nabla \cdot \boldsymbol{v}$. Here in turn P is the function space containing the virtual displacement field $\boldsymbol{w}[\boldsymbol{x}]$, and S is the function space containing the virtual fluid pressure field $\eta[\boldsymbol{x}]$. We also introduced prescribed nominal traction $\bar{\boldsymbol{t}}_1$ and flow Q on the outer surface Γ_0.

The next step is to establish the set of discretized finite element equations pertinent to the present choice of interpolation of displacements and fluid pressure. In view of the weak form of momentum and mass balances (2.45)–(2.46) we obtain

$$\left[\delta \hat{\boldsymbol{u}}^t, \delta \hat{\boldsymbol{p}}^t \right] \overset{\text{NEL}}{\underset{e=1}{A}} \begin{bmatrix} \boldsymbol{b}_e - \boldsymbol{f}_e^{\text{ext}} \\ \boldsymbol{c}_e \end{bmatrix} = 0, \tag{2.47}$$

where explicit expressions for the unbalances $\boldsymbol{b}_e - \boldsymbol{f}_e^{\text{ext}}$ and $\boldsymbol{c}_e$ are obtained as

$$\begin{aligned} \boldsymbol{b}_e - \boldsymbol{f}_e^{\text{ext}} &= \int_{D_{0e}} \left(\boldsymbol{B}_u^e \right)^t \left(\hat{\boldsymbol{\tau}} - J p \hat{\mathbf{1}} \right) dV + \int_{\Gamma_e} \bar{p} \left(\hat{\boldsymbol{N}}_u^e \right)^t \boldsymbol{n}[s] \text{ds}, \\ \boldsymbol{c}_e &= \int_{D_{0e}} \left[\left(\hat{\boldsymbol{N}}_p^e \right)^t \left(J - {}^n J \right) + J \left(\hat{\boldsymbol{N}}_p^e \right)^t \frac{\Delta t n^f}{\rho^f} \left((1-\xi) k^g q - \left(\rho^l - \rho^g \right) \dot{\xi} \right) \right] dV - \\ &\quad \int_{D_{0e}} J \left[\left(\hat{\boldsymbol{N}}_p^e \right)^t \left(n_0^s e^{\varepsilon_v^s} \Delta \varepsilon_v^s \right) - \frac{\Delta t}{\xi} \left(\boldsymbol{B}_p^e \right)^t \boldsymbol{v}^d \right] dV + \int_{\Gamma_e} \left(\hat{\boldsymbol{N}}_p^e \right)^t \Delta t Q d\Gamma, \end{aligned} \tag{2.48}$$

where $\bar{p}$ denotes the prescribed pressure on the external boundary.

3 Summary of Appended Papers

Paper A The aim of this formulation was to model the resin wet out through the highly deformable fiber preform when the resin flow is coupled to the preform deformation. The challenges that are considered to be modelled are (1) the highly deformable preform and its shape due to the interaction between the external pressure loading and the intrinsic fluid pressure and (2) the flow front tracking of the resin infiltration into the fiber preform. To be able to handle these challenges a compressible two–phase porous media formulation is put forward involving an additional liquid mass balance relationship as compared to the standard compressible porous media formulation. In other word, a saturation degree concept based on the additional liquid mass balance relationship has been added to the two–phase porous media theory were compressible continuum formulation is traversing into incompressibility with increasing partial saturation degree. In this contribution, we have developed the existing two phase porous media theory further, in such a way to simulate the popular infusion processes. Examples of vacuum infusion and resin transfer molding were simulated and sensitivity analysis with respect to time step and mesh size are also studied.

Paper B In this contribution the aim was to handle the challenges that might arise during RTM, Vacuum Assisted Resin Infusion (VARI) and Vacuum Bag Only (VBO) prepregs, such as the preform deformation, resin wet out in a partially filled fiber network, micro–infiltration through the fiber plies and intrinsic compressibility in the solid phase. In addition, development of an anisotropic deformation dependent permeability model pertinent to the dual scale resin flow was established. Towards the development of this framework for process modeling of composite manufacturing, we established a finite element based formulation in order to simulate coupled dual scale flow through the fibrous preforms using the two–phase porous media theory. In order to numerically test the framework we consider a compressive relaxation test applied to a fluid filled fiber network, which is related to press forming of VBO prepregs. Number of simulation was carried out regarding two different boundary conditions, partially drained and globally undrained, and then results were compared with respect to reaction forces and microscopic saturation. The effect of compaction on the anisotropic permeability model was also studied.

Paper C In this contribution we had the possibility of having an experimental verification of the modeled generic algorithm in Paper B. Initially the aim was to assess the sub–models that were developed within the presented two–phase continuum mechanical FE framework in Paper B for press forming manufacturing processes. Unfortunately, experimental methods capable of parameter characterization for some of the competing processes are not existing and needs to be developed. Nevertheless, the models were placed in context with an experimental method, employed to study the preform deformations considered separated from other sub–processes. This experiment consisted of deforming the specimen at increasing levels of displacement, and at each increment, the displacement

is held constant until the measured load relaxes to a stable value. Finally, to relate the FE–framework to the material response calibrations and model validations were carried out against the relaxation experiment.

Paper D In the present paper we present a novel finite element method capable of handling most of the physics arising in the resin wet–out step for any composite system and processing case. The ultimate goal of this contribution is to establish an unified generic and general simulation tool for structural (long fiber) composite processing where, to this date, there is no single FE based tool available commercially for this purpose. To achieve this goal a compressible two–phase continuum formulation where a key feature is to model the involved physics via innovative use of the compressibility of the phases has been put forward. The idea of this simulation tool is to give the user the option to choose the boundary conditions, initial conditions and material data depending on the process (s)he has in mind to simulate, whereas the core in the method is to solve the time–dependent dual–scale compressible resin infiltration problem through the fiber preform assumed as a compressible volumetrically–deformable porous material. Different deformation dependent permeability models are also in place to choose from, depending on the type of the process and also the type of the preform (isotropic or anisotropic). At the end, the routine was tested for infusion family and compression molding processes and the respective results were compared to those obtained in Paper A and Paper B.

4 Conclusion

The focus of this PhD thesis was on the development of a holistic modeling of composite manufacturing. Manufacturing techniques that are considered in this study were wide range of advanced manufacturing methods. For example, Liquid Resin Infusion (LRI) family is one, where in Paper A and Paper D we have shown different simulation examples for resin infusion and Resin Transfer Molding (RTM) based on different formulations. The other one is Out of Autoclave (OoA) family. We can see examples of press forming and Vacuum Bag Only (VBO) prepregs in Paper B and Paper D.

The model proposed in this thesis for our objective was based on the development of the theory of two–phase porous media where introducing the phase compressibility has enhanced the ability of the model to capture different physical sub–processes in different scale. In that sense, we have developed a special binary porous media formulation in order to model a dual–scale coupled flow–deformation process with constitutive relations concerning different mechanisms governing all the processes involving (1) constitutive effective stress response of the fiber bed, (2) Darcy law governing the macroscopic interaction between the two phases, (3) isotropic/anisotropic deformation–dependent permeability, (4) compressible liquid–gas response, and (5) solid compaction and micro–infiltration of resin into fiber plies. In addition, if necessary, the model accounts for the non–saturated behaviour typical for the transition region at the flow front between full and non–saturation.

Phase compressibility was introduced, first, in Paper A where the pore fluid was considered to consist of incompressible liquid and highly compressible gas phase. The

formulation of the compressible liquid–gas response led us to the evolution of the saturation degree where we could establish a continuum–based model to identify the flow front of the moving resin into the porous media. Later in Paper B, we introduced the solid compressibility to be able to address the elastic packing response of the fiber plies. Finally, in Paper D in the formulation of mass balance we considered both phases, solid and fluid, compressible. The ultimate goal was to establish a framework where the competing and interrelated sub–processes, mentioned above, in different temporal and spatial scale, could be captured in a single FE formulation routine.

The complexity in the handling of this model stems from highly non–linear problem solved by finite element. This is due to non–linear kinematics, related to material behavior of the different phases and time scales, which at the same time are interacting during the process. There is also a dependency of the routine on material parameters. In Paper C we have tried to experimentally asses some of the sub–processes occurring during the OoA processes and characterize some of the uncertain data to fit them to the model. However, lack of consistent experimental methods for characterization of the material has limited the study and is a subject for further research in this field.

5 Future work

Process modeling of composite manufacturing is subjected to change every day by inventing new manufacturing techniques, new materials, new facilities, etc. So there will always be research issues to be considered with respect to physical phenomena which are involved with the processes. In respect to the developments in this contribution, there are number of concerns that are interesting and can be subjected for further improvement in the future.

- The dependency of the current method on time stepping through numerical implementation is one major issue to be considered. Development of a routine to calculate the time step in such a way to be applicable for both time and spatial scale without crashing the simulation is desired.
- Development of modules for considering curing and residual stresses will complete the holistic approach modeling algorithm.
- The formulation of the governing equation, i.e. the extra mass balance for the liquid phase, when we are dealing with the flow front tracking problem needs to be reconsidered. The flow front distribution as a smeared flow front is not representing the real physical concept.
- Experimental study of the sub processes are of interest. However, experimental methods capable of parameter characterization for some of the competing processes are not existing and needs to be developed, which is, as a matter of fact, an ongoing effort within our group.
- So far, the simulation routine is a single finite element formulation using a quadratic six node triangular element. Further development of the implementation where other types of higher order elements can be used is a must.
- The simulation is capable of handling two dimensional simulations. implementation of 3D elements to the formulation will widen the range of the application.

References

[1] F. Trochu et al. "Advanced numerical simulation of liquid composite molding for process analysis and optimization". In: *Composites Part A: applied science and manufacturing* 37.6 (2006), pp. 890–902.

[2] R. S. Parnas. "Liquid composite molding". In: *Hanser Gardner Publications* (2000).

[3] W. D. Callister. *Materials Science and Engineering An Introduction*. India: John Wiley & Sons, Inc., 2007. ISBN: 978-0-471-73696-7.

[4] F. L. Matthews et al. *Finite element modelling of composite materials and structures*. Cambridge, England: WoodHead Publishing Limited, 2000. ISBN: 978-1-85573-422-7.

[5] B. D. Agarwal, L. J. Broutman, and K. Chandrashekhara. *Analysis and performance of fiber composites*. John Wiley and Sons, Inc., 2006. ISBN: 978-0-471-26891-8.

[6] G. D. Vita, R. Ferraro, and P. Perugini. "Development of Process Simulation Models for Composite Technology". In: *Materials and Manufacturing Processes* 10.1 (1995), pp. 103–113.

[7] S. G. Advani and E. M. Sozer. *Process Modeling in Composites Manufacturing*. New York • Basel: Marcel Dekker, Inc., 2010. ISBN: 978-1420090826.

[8] P. Simacek and S. G. Advani. "Desirable features in mold filling simulations for liquid molding processes". In: *Journal of Polymer Composites* 25.4 (2004), pp. 355–367.

[9] W. Ehlers and J. Bluhm. *Porous Media, Theory, Experiments and Numerical Applications*. Springer–Verlag Berlin Heidelberg New York, 2002. ISBN: 3-540-43763-0.

[10] L. J. Gibson. "Bimechanics of cellular solid". In: *Journal of Biomechanics* 38.3 (2005), pp. 377–399.

[11] R. Larsson, M. S. Rouhi, and M. Wysocki. "Free surface flow and preform deformation in composites manufacturing based on porous media theory". In: *European Journal of Mechanics A/Solids* 31.1 (2012), pp. 1–12.

[12] M. S. Rouhi, M. Wysocki, and R. Larsson. "Modeling of coupled dual-scale flow–deformation processes in composites manufacturing". In: *Journal of Composites Part A: applied science and manufacturing* 46 (2013), pp. 108–116.

[13] K. M. Pillai, C. L. Tucker, and F. N. Phelan. "Numerical Simulation of Injection/Compression Liquid Composite Moulding. Part 2: Preform Compression". In: *Journal of Composites Part A: applied science and manufacturing* 32 (2001), pp. 207–220.

[14] R. Larsson, M. Wysocki, and S. Toll. "Process–modelling of composites using two–phase porous media theory". In: *European Journal of Mechanics. A/Solids* 23.1 (2004), pp. 15–36.

[15] S. Toll. "Packing Mechanics of Fiber Reinforcement". In: *Polymer Engineering and Science* 38.8 (1998), pp. 1337–1350.

[16] B. R. Gebart. "Permeability of unidirectional reinforcements for RTM". In: *Journal of Composite Materials* 26.8 (1992), pp. 1100–1113.

[17] B. T. Astrom. *Manufacturing of Polymer Composites*. London: Chapman and Hall, 1997. ISBN: 0412819600.